NANO LETTERS
Letter
Cite This: Nano Lett. XXXX, XXX, XXX−XXX
pubs.acs.org/NanoLett

Neighboring Pt Atom Sites in an Ultrathin FePt Nanosheet for the Efficient and Highly CO-Tolerant Oxygen Reduction Reaction

Wenlong Chen,[†,#] Wenpei Gao,[‡] Peng Tu,[§] Tom Robert,[†] Yanling Ma,[†,#] Hao Shan,[†,#] Xin Gu,[†] Wen Shang,[†] Peng Tao,[†] Chengyi Song,[†] Tao Deng,[†,#] Hong Zhu,*[,§] Xiaoqing Pan,*[,‡,∥] Hong Yang,[⊥] and Jianbo Wu*[,†,#]

[†]State Key Laboratory of Metal Matrix Composites, School of Materials Science and Engineering, Shanghai Jiao Tong University, 800 Dongchuan Rd, Shanghai, 200240, People's Republic of China

[‡]Department of Chemical Engineering and Materials Science, University of California, Irvine, Irvine, California 92697, United States

[§]University of Michigan−Shanghai Jiao Tong University Joint Institute, Shanghai Jiao Tong University, 800 Dongchuan Road, Shanghai 200240, People's Republic of China

[∥]Department of Physics and Astronomy, University of California, Irvine, Irvine, California 92697, United States

[⊥]Department of Chemical & Biomolecular Engineering, University of Illinois at Urbana−Champaign, 206 Roger Adams Laboratory, MC-712, 600 South Mathews Avenue, Urbana, Illinois 61801, United States

[#]Hydrogen Science Research Center, Shanghai Jiao Tong University, 800 Dongchuan Rd, Shanghai 200240, People's Republic of China

Supporting Information

ABSTRACT: Single atom catalyst and ultrathin two-dimensional (2D) nanostructures exhibit improved properties because of the improved exposure of more active atomic sites and optimized electronic structures. However, the oxygen reduction reaction (ORR) in fuel cells via a fast four-electron path usually uses at least two Pt atoms, which cannot be realized in highly isolated single Pt atoms. The synthesis of a densely dispersed single atom catalyst with adjacent atoms accessible at the same time on a matrix with a high surface area provides a feasible way and, however, is challenging. Here, we synthesize ultrathin FePt nanosheets (NSs) with 6.7 wt % neighboring dispersed Pt atoms. Different from the reported isolated Pt single atom catalysts, these ultrathin wrinkled FePt NSs with neighboring Pt sites adopt a four-electron reduction pathway, a high electrochemical active surface area (ECSA) of 545.54 $m^2 g_{Pt}^{-1}$, and an improved mass activity 7 times as high as Pt/C in the ORR. The improved performance results from the optimal use of neighboring Pt atoms dispersed in a more packed spacing and exposed on the surface of ultrathin sheets. The Pt atoms can interact synergistically to catalyze a fast ORR process. Furthermore, both the experiment and density functional theory (DFT) calculation indicated an outstanding CO-tolerance performance of this catalyst in the ORR.

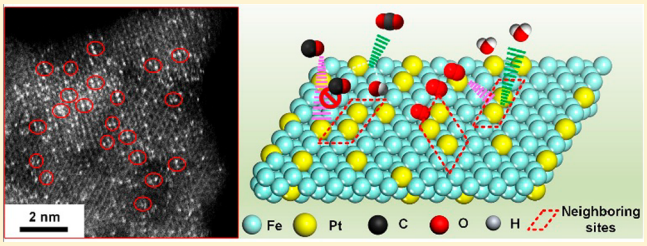

KEYWORDS: *Oxygen reduction reaction, FePt nanosheets, CO tolerance, atomically dispersed catalyst, electrochemistry, neighboring platinum atoms*

The morphology and shape anisotropy of a nanoparticle catalyst can largely affect its selectivity and activity.[1] For the catalyst in ORR, whose slow kinetics is one of the most crucial limiting factors for commercialization of proton exchange membrane fuel cells (PEMFCs),[2,3] tailoring the geometries of metallic nanostructures is thus essential to achieve a high catalytic performance.[4,5] The possibility of synthesizing 2D metal catalysts represents a new paradigm in optimization of the activity and selectivity because such structure offers a larger surface area with active sites for a catalytic reaction to occur and a faster electron transport than their one-dimensional (1D) and three-dimensional (3D) counterparts, such as nanospheres, faceted nanocrystals, nanorods, and nanowires.[6,7] 2D structures also have additional advantageous mechanical and electronic properties as demonstrated in a variety of inorganic 2D compounds.[8,9] These properties are the bases for diverse potential applications of 2D nanomaterials in catalysis,[1,10,11] energy harvesting and energy storage,[12,13] biological sensing,[14] and electronic devices.[15] Furthermore, 2D materials of the thickness of several atomic layers may also utilize nearly all of the atoms for catalytic reaction due to the ultrathin thickness.

However, the synthesis of 2D metallic nanostructures is often challenging: 2D structures usually require a weak

Received: June 27, 2018
Revised: July 18, 2018
Published: July 31, 2018

DOI: 10.1021/acs.nanolett.8b02606
Nano Lett. XXXX, XXX, XXX−XXX

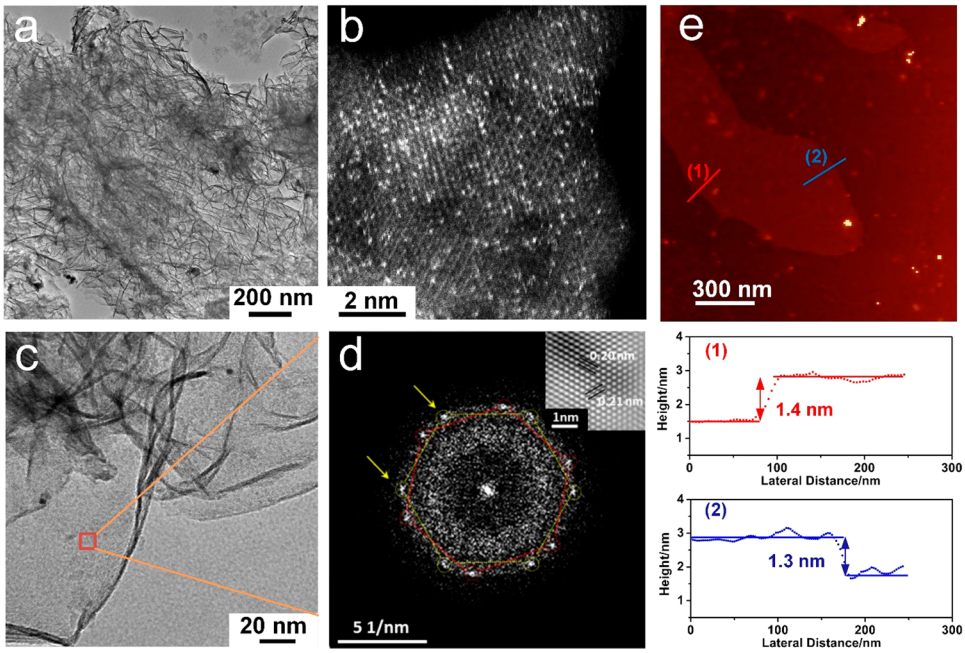

Figure 1. Representative view of (a) TEM, (b) HAADF-STEM, (c) high-magnification TEM, and (d) diffractogram images using fast Fourier transformation from the selected red square area in panel c. The FFT pattern shows two sets of diffraction spots form the Fe (111) zone axis. The inset in panel d shows the inverse FFT image using the selected set of spots indicated by the yellow arrows. (e) AFM image and the corresponding height profiles of the FePt NS.

interaction between layers and strong bonding within a layer at the atomic scale,[16] which is often seen in semiconductor materials,[16] such as graphene, CN,[17] WS_2,[13] MoS_2,[18,19] Co_3O_4,[11] and $MoSe_2$.[20] Generally, metal atoms favor 3D growth due to the nature of a metallic bond. So far, 2D metal or alloy structures have been successfully made only from noble metals such as Rh,[16,21] Pd,[22,23] Ru,[24] Au,[25] Pt−Cu,[26,27] Pd@PtM,[28] and PtPb/Pt[29] in the forms of either nanoplate or nanosheet, which have been reported active in the oxidation of ethanol, methanol, formic acid, and other catalytic reactions.[26,28,30] Nevertheless, a few noble metal-based 2D nanostructures have been reported as catalysts for the ORR. Only very recently, core−shell PtPb nanoplates have been reported active for the ORR.[29] As the thickness of the plates is more than 5 nm, the properties are more close to 3D structures. The activity improvement is mostly due to the biaxial strain from the Pt shell, similar to the surface compressive strain enhanced activity reported on 3D core−shell nanoparticles.[31−35] One obstacle for developing a 2D ORR catalyst is that the 2D structures have a high tendency to stack, causing the loss of surface area; however, a lower thickness (less than 10 atomic layers) must be preserved to make optimal use of active atoms. One possible solution is to crumple 2D structures with wrinkles to avoid the stack of sheets and preserve active sites.[23,36,37]

In the past few years, the possibility of synthesizing single metal atom systems also enables optimization of the activity and selectivity of catalysts.[38−40] Single atom catalysts show an improved cost efficiency because almost all atoms participate in the reaction. However, the low loading of a single atom to limit the aggregation also hinders the availability of enough active sites for reactants or intermediates in some catalytic reactions, such as the ORR, whose fast four-electron reduction needs at least two neighboring Pt atomic sites to participate. The isolated single Pt atoms usually resulted from the low Pt mass loading (<2%) and, on the other hand, usually proceed with a slower two-electron path for ORR.[41] Because of the sintering of atoms, synthesizing an atomically dispersed catalyst with a high loading remains challenging. Only a few works have reported the high atom loading or dimers catalysts.[42,43] For example, Choi et al. used the highly functionalized carbon to support Pt single atoms at a high loading of 5 wt %. Because the sulfur functionality species are strongly adsorbed on Pt, the oxygen is still reduced into H_2O_2 via a two-electron path.[42] On the other hand, while lots of Pt-based catalysts have already been shown to exhibit an improved activity, another long-standing issue on CO tolerance for the ORR becomes a major limitation for practical utilization of fuel cells.[40,44−48] Because of the strong adsorption of CO on noble metal, these ORR catalysts are likely poisoned by the existence of CO during reaction, for example, using air and H_2 with even 0.001 vol % CO impurity as the oxygen and fuel resources could lead to the activity loss.[44,49,50] Currently, there are a few reports on CO poisoning during the ORR. Hence, it is also urgent to search for high CO-tolerant catalysts for fuel cells.

In this work, we developed a CO-assisted method to prepare an ultrathin 2D wrinkled FePt nanosheet (NS) catalyst with ∼6.7 wt % "neighboring Pt"; the high loading provides densely dispersed Pt atoms neighboring each other on a large surface, offering an excellent electrocatalytic activity and high CO-tolerant ability. The as-synthesized FePt NSs were only 5−6 atomic layers thick (1.2 nm in thickness), with Pt atoms on the wrinkled surfaces. The surface wrinkling can preserve the high surface area and efficiently expose the active Pt sites,[23,36,37] thus enhancing the ORR activity. The "neighboring atom catalyst" not only reserves the advantages of the traditional single atom catalysts but also can synergistically catalyze the reaction, which needs two or more nearby sites, contributing to a four-electron pathway of the ORR, which is very different from the previous reported isolated single Pt atom catalysts

DOI: 10.1021/acs.nanolett.8b02606
Nano Lett. XXXX, XXX, XXX−XXX

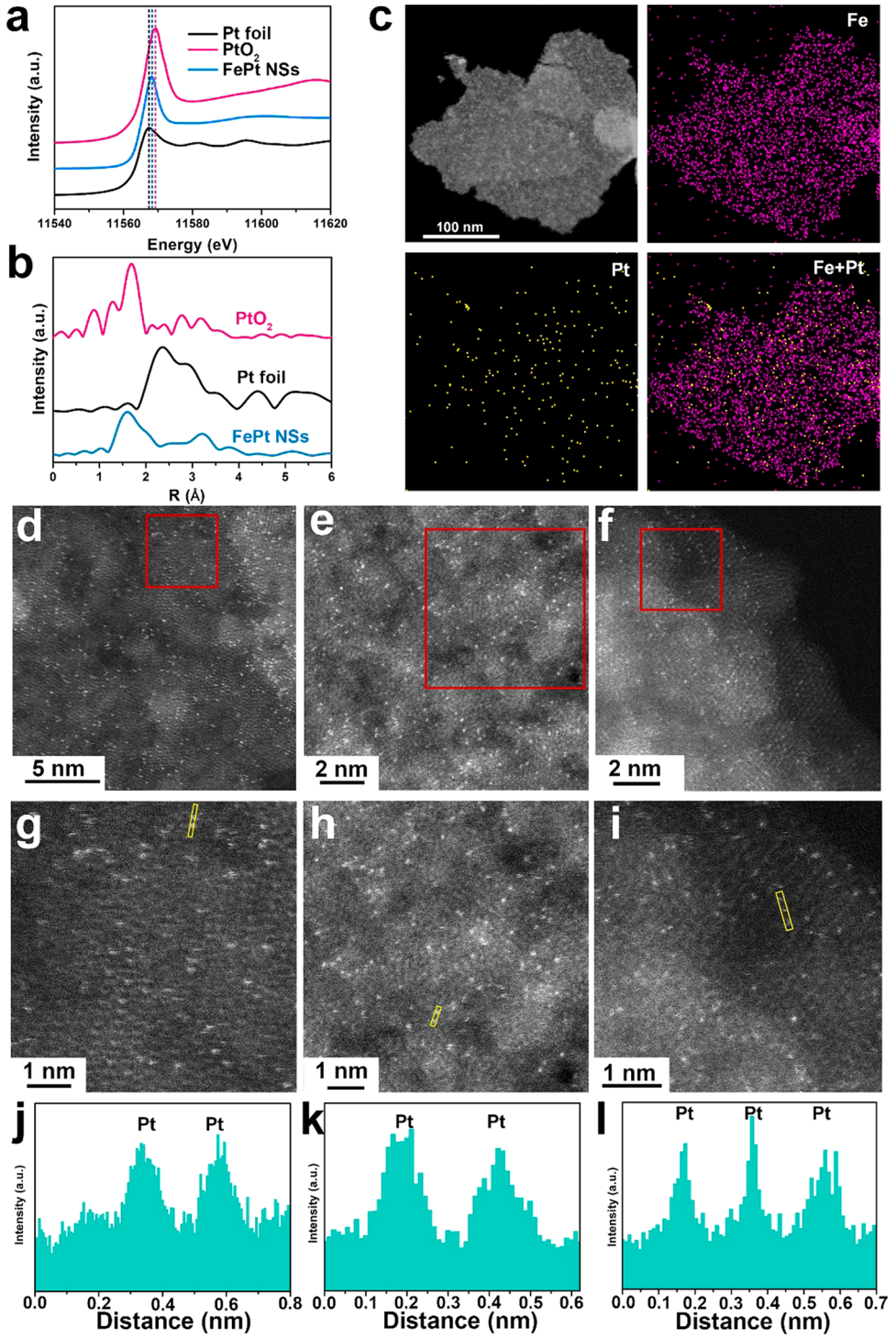

Figure 2. (a) Pt L_3-edge XANES of the FePt NSs, Pt foil, and PtO_2 samples. (b) Fourier transforms of k^3-weighted Pt L_3-edge EXAFS. (c) Typical HAADF-STEM image and STEM-EDX elemental maps of Fe, Pt, and overlay of the FePt NSs. (d–f) Aberration-corrected HAADF-STEM images of the neighboring atom dispersion of Pt in the FePt NSs from different regions. (g–i) Magnified HAADF images of the red rectangle regions in parts d, e, and f, respectively. (j–l) Line-scanning intensity profile obtained from the area highlighted with yellow rectangles in parts g–i, correspondingly.

that usually showed a two-electron path to produce H_2O_2. The use of Fe as a non-Pt group metal (PGM) as a supporting alloy matrix could suppress CO poisoning by modifying the Pt electronic structure that weakened the Pt–CO bond and also could facilitate the CO oxidation by more OH groups absorbed on nearby Fe, thus accelerating the elimination of the CO intermediates.[51−53]

Results and Discussion. The FePt NSs were synthesized based on a surfactant-free solvothermal method assisted with a Schlenk line. The sheets spread continuously more than 100 nm in lateral dimension (Figure 1a) and were flexible in structure with wrinkles as shown by the dark strikes in the TEM image (Figure 1a and Figure S1). The low-magnification TEM in Figure 1a and scanning electron microscopy (SEM)

DOI: 10.1021/acs.nanolett.8b02606
Nano Lett. XXXX, XXX, XXX−XXX

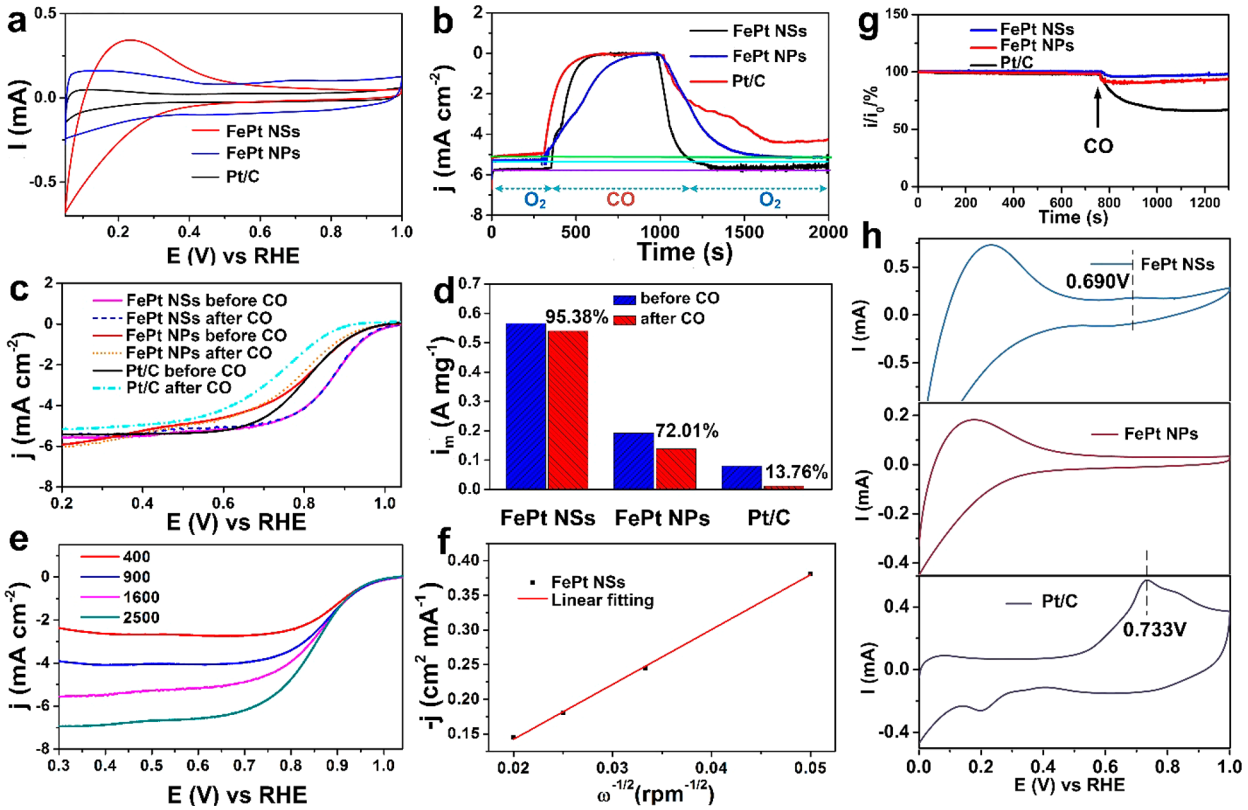

Figure 3. (a) CV curves of FePt NSs, NPs, and Pt/C. (b) *i*−*t* curves with O_2 bubbling or CO bubbling during the test of the catalysts at the potential of 0.1 V. (c) ORR polarization curves of different catalysts before and after CO-tolerance measurements. (d) The mass activities for comparison at 0.9 V before and after CO-tolerance measurements for the three catalysts. (e) RDE curves for the ORR of FePt NSs electrocatalyst at various rotation rates, and (f) Koutecky−Levich plots of the rotating disk current at 0.3 V. (g) CO-poison effect on the *i*−*t* chronoamperometric response for different electrodes in the presence of oxygen. The arrow indicates the addition of ∼10% (volume/volume vs O_2) CO gas was introduced into the O_2-saturated 0.1 M KOH electrochemical cell. i_0, initial current at 0.1 V. (h) CO stripping curves of the three catalysts.

image in Figure S1 indicated the high yield of FePt nanosheets. In the high-angle annular dark-field (HAADF) aberration-corrected scanning transmission electron microscopy (Cs-STEM) images of the nanosheet (Figure 1b), the highly dispersed locations of brighter spots on the darker matrix revealed the abundant neighboring and the high density of atomically dispersed Pt in the FePt alloy sheets. Figure 1a−c showed almost no obvious nanoparticles or big clusters, indicating Pt is incorporated into the Fe matrix in the form of a single atom. The typical thickness of the FePt NSs measured by atomic force microscopy (AFM) was below 2 nm (Figure 1e). High-resolution TEM indicates the width of a side wall around 1.2 nm, which corresponds to the thickness from 5 to 6 atomic layers (Figure S2). The atomically thin layers make it possible to expose the active Pt sites efficiently. The diffraction spots from the fast Fourier transformation (FFT) of the HRTEM image (Figure 1d) indicated that the ultrathin FePt NSs had (111) basal planes. In the image by inverse FFT using the selected set of diffraction spots (inset in Figure 1d), the two intersected lattices show the d spacing of 0.20 and 0.21 nm, corresponding to the Fe {111} planes. The X-ray diffraction (XRD) (Figure S3) of the finally collected powder sample shows mainly the Fe peaks because the noncrystalline nature of a low percentage of Pt content does not form a peak in XRD.[40] Henceforth, based on the HAADF images and XRD, the as-prepared FePt NSs primarily show the densely dispersed Pt atoms in FePt 2D wrinkle nanosheets.

To further explore the detailed state of Pt in the FePt nanosheet, we studied the X-ray absorption spectroscopy (XAS) to investigate the electronic structure. Figure 2a shows the X-ray absorption near-edge structure (XANES) of the FePt NSs, at the Pt L_3-edge. Pt foil and PtO_2 are shown as references. The XANES white line peaks of the FePt NSs are located between the Pt^0 from Pt foil and Pt^{4+} from PtO_2, indicating the Pt in FePt NSs was in an oxidation state between Pt^0 and Pt^{4+}. The intensity of the white line peaks also followed the sequence of PtO_2 > FePt NSs > Pt foil. The extended X-ray absorption fine structure (EXAFS) in Figure 2b showed the difference between FePt NSs, Pt foil, and PtO_2 clearly: the Pt−Pt coordination numbers for Pt foil and PtO_2 were estimated to be ∼12 and 6, while that for FePt NSs is not obvious and negligible. In Pt foil, the peak at ∼2.7 Å corresponds to the Pt−Pt bond typical for the Pt foil and Pt nanoparticle samples.[54] This is different from that of FePt NSs, where Pt is atomically dispersed without obvious peaks from the Pt−Pt bond, indicating the absence of Pt particles in FePt NSs.[43] The first shell peak in the Fourier transform (FT) spectrum of FePt NSs at ∼1.7 Å is similar to the peak at ∼1.9 Å of PtO_2, which can be assigned to the Pt−O bond, in correspondence with their oxidation state. The peak in ∼2.5 Å for the FePt NSs is from the Pt−Fe bond length, and the peak in ∼3.1 Å is the bond length of the second nearest shell of Fe with Pt.[54] In addition, energy dispersive spectroscopy (EDS) elemental mapping demonstrates that Fe and Pt are uniformly distributed across large areas of the FePt NSs (Figure 2c and Figure S4).

DOI: 10.1021/acs.nanolett.8b02606
Nano Lett. XXXX, XXX, XXX−XXX

These results indicated again that the Pt in the FePt NS catalyst does not form Pt nanoparticles but is atomically dispersed. From the HAADF STEM image for multiple regions of the NS (Figure 2d–i), the dispersion of Pt atom is highly dense, and most of the atoms neighbor several other Pt atoms. This is different from the traditional single atom catalysts where each atom is far away from others. From the intensity line profiles, Pt atoms are neighbored by 0.24, 0.23, and 0.20 nm in distance (Figure 2j–l), respectively, with an average of 0.22 nm, similar to the atom–atom spacing of Pt in the (111) plane. For comparison, reported isolated single atoms are usually separated by >1 nm.[38,40,41] Henceforth, although the Pt atoms are atomically dispersed in the nanosheets, the atoms are neighbored densely and could still interact with the nearby Pt efficiently. The neighboring Pt atoms can both be accessed by the same oxygen molecule.

Based on the Brunauer–Emmett–Teller (BET) method (Figure S5), we measured the specific surface area of FePt NSs as 158.779 $m^2\ g^{-1}$, a high value for surface area. The Fe/Pt atomic ratios of the as-prepared nanosheets were 97:3 from EDS elemental analysis (Figure S6) and 98:2 from inductively coupled plasma mass spectrometry (ICP-AES in Table S1). The shape evolution of FePt NSs during the synthesis, effects of the ratio between precursors, and effect of solvent on morphology of the alloy products were also investigated (detailed information and further discussion in the Supporting Information and Figure S7–S11). The detailed study indicated that only under the proper synthetic condition including the precursor's ratio of 1:10 (Pt/Fe), using the solvent of EG and the reaction time of 42 h, thin FePt NSs can be collected. Otherwise, for example, when the solvent was changed from EG to DMF, the FePt products turned into nanoparticles (FePt NPs) even though its composition ($Fe_{97}Pt_3$) remained almost unchanged (Figure S4 and S10). In comparison to the BET surface area of 158.779 $m^2\ g^{-1}$ from the FePt NSs, the BET surface area of the nanoparticles was 70.668 $m^2\ g^{-1}$, close to the ECSA of Pt/C (Figure S5).

As these ultrathin FePt NSs expose atomically dispersed neighboring Pt, which can access the same oxygen molecule during electrochemical reaction, we expect improved performances from the ORR catalysis. The FePt NSs, FePt NPs, and Pt/C were loaded on a glassy carbon rotating disk electrode (RDE), and the ORR measurements were carried out in a three-electrode system. The cyclic voltammograms in Figure 3a were used to measure the ECSA. The normalized ECSAs to total metal mass are 36.37, 9.16, and 42.19 $m^2\ g_{metal}^{-1}$ for FePt NSs, FePt NPs, and Pt/C, respectively. As Pt atoms sites are the most active during catalysis, the ECSA of Pt species in FePt NSs based on the Pt mass ratio (6.7%) achieves 545.54 $m^2\ g_{Pt}^{-1}$. The specific surface activity (i_s) is 0.104, 0.158, and 0.190 mA cm_{Pt}^{-2} for FePt NSs, FePt NPs, and Pt/C at 0.9 V, respectively (Table S2). The mass activities (i_m) of FePt NSs, FePt NPs, and Pt/C are 0.566, 0.192, and 0.080 A mg_{Pt}^{-1}, correspondingly. It indicates that an extremely low amount of Pt with well atomic dispersion on FePt NSs showed almost 7 times as high ORR mass activity as that of Pt/C. Notably, the promoted catalytic activity could be ascribed to the enhanced 2D electronic conductivity, the faster charge transfer, and the better accessibility to the increased number of catalytically active atomic sites on the 2D wrinkled structure.[55] The ultrathin thickness down to a few atomic layers endows the FePt sheets with a large portion of active atoms on the surface. The largely improved ECSA of 545.54 $m^2\ g_{Pt}^{-1}$ of FePt NSs is nearly half of the real surface area (RSA) of a freestanding Pt single atom and similar to the RSA of a supported Pt single atom.[41,56] (See the calculation details on the estimation of surface area of a Pt single atom in Supporting Information.) This indicates that the Pt sites are efficiently exposed at the surface of the ultrathin few-atom-layer NSs and are accessible in the reaction of oxygen reduction, in agreement with the HAADF STEM in Figure 1b and Figure 2. This feature makes it possible for the ultrahigh ECSA. In addition, the improved conductivity of 2D structure could allow for faster electron transport within the Fe layers, which is beneficial to the reduction reaction process.

The electrocatalytic activity of the FePt NS catalysts was quantitatively examined as a function of rotation speed of the rotating disk electrode ranging from 400 to 2500 rpm to investigate the number of electron transfer involved in the ORR, as can be seen in Figure 3e,f. Figure 3e shows the ORR polarization curves of the FePt NSs recorded at different rotation speeds, and the corresponding Koutechky–Levich plots were shown in Figure 3f. The plot shows a good linearity, indicating first-order reaction kinetics toward dissolved oxygen and a similar electron-transfer number (n) during the ORR process.[57] Based on the values calculated from the plot, n is calculated to be 3.67, indicating the FePt NSs exhibit a four-electron transfer pathway. In contrast, usually for the very low loading and isolated Pt single atom catalysts, they catalyzed the ORR process by a two-electron path because the fast four-electron path needs at least two or more nearby atoms to cooperate as active sites to cleave the O_2 and catalyze the reaction.[41] These results also proved that Pt is atomically dispersed in a high density and that the individual Pt atoms are neighbored by other Pt atoms within a short distance. As mentioned above, most of the Pt atoms were nearby to each other (Figure 2), in the form of dimers, trimers, or multiatoms. Henceforth, this unique structure makes the sufficient utilization of active Pt atoms and, meanwhile, still provides sites with adjacent Pt atoms, which are required to break the O–O bond via the fast ORR path. The electrochemical durability of the FePt NSs for long-term use was also evaluated by accelerated durability tests (ADT) under the potential between 0.6 and 1.0 V in Ar-saturated 0.1 M KOH solution. Figure S12a,b showed the ORR curves of FePt NS and Pt/C catalysts before and after 20 000 cycles, respectively. The durability results (Table S2) showed that the FePt NSs still held 73.9% mass activity, while that of the Pt/C was only 33.8%, indicating a high stability performance of the neighboring Pt atom FePt NS catalyst. We further investigated the morphology of the atomically dispersed FePt NSs using HAADF-STEM after the stability test (Figure S13a). As a result, the neighboring atomic dispersion of Pt was still well-maintained (Figure S13), which agreed with its good stability in the ORR performance.

CO poisoning occurs on most catalysts, which blocks active sites of the catalysts.[44,58,50] As the current Pt-based catalyst has already met the criteria of commercialization based on the achieved activity, activity degradation due to CO poisoning in the ORR becomes a major limitation. The effect of CO on the electrocatalytic activity of the FePt NS electrode was investigated here. O_2 and CO gas flow was bubbled alternately into the electrolyte, with the chronoamperometric method being applied in the whole process to track the current dynamic change (Figure 3b).[59] After the solution was saturated with O_2, all of the three catalyst curves showed steady limited

DOI: 10.1021/acs.nanolett.8b02606
Nano Lett. XXXX, XXX, XXX–XXX

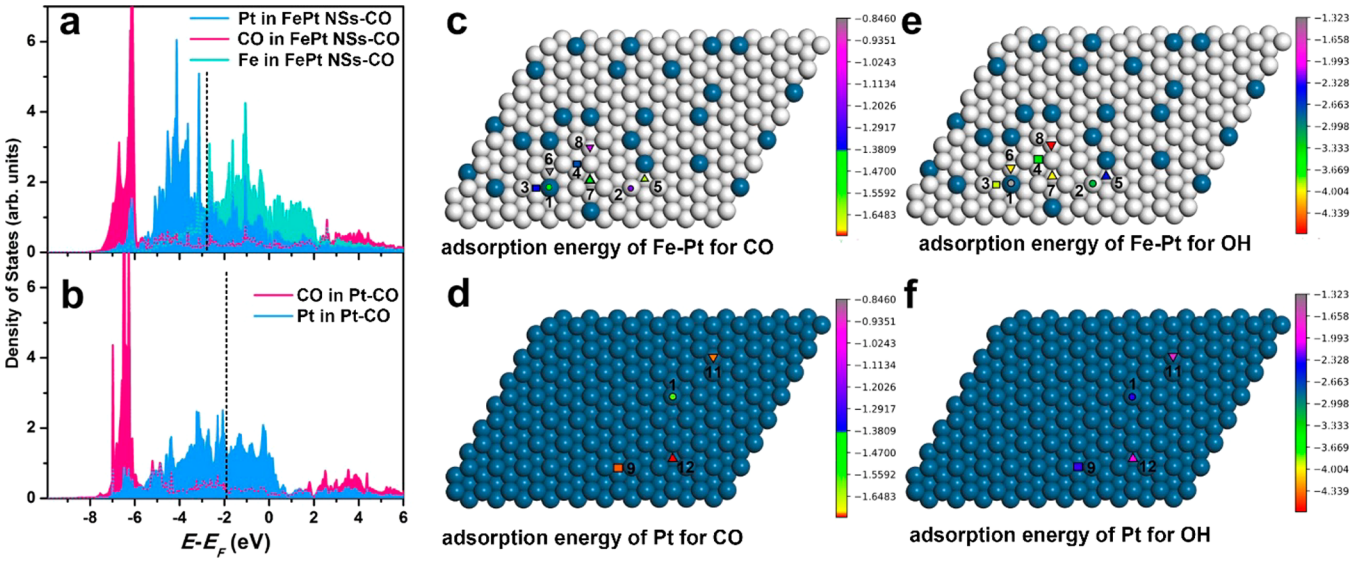

Figure 4. DFT calculations. (a, b) The density of states of adsorbates and Fe or Pt atoms directly bonded to adsorbates at the most stable adsorption site on the FePt NS surface and Pt surface. The d band center (vertical dashed line) of Pt atoms of FePt NSs is a negative shift than that of Pt. (c, d) The calculated binding energies for CO on FePt (111) and Pt (111) on various adsorption sites, relative to the lowest binding energy, and (e, f) the calculated binding energies for OH on FePt (111) and Pt (111) on various adsorption sites, relative to the lowest binding energy. The blue ball represents a Pt atom, and the white ball represents an Fe atom. The different shapes with numbers represent different adsorption sites.

currents. The initial limited current of FePt NSs was 5.72 mA cm^{-2}, the FePt NPs was 5.27 mA cm^{-2}, and the value for Pt/C was 5.18 mA cm^{-2}. After the bubbling gas was switched to CO, all of the current densities of the three electrodes went down to near zero rapidly and kept steady because, in the presence of the CO, the active Pt surface was blocked for oxygen reduction. Subsequently, when the bubbled gas was switched from CO to O_2, the limited currents of all catalysts increased immediately. However, after the resaturation of O_2, the recovery of the limited currents for the three electrodes showed a big difference. As shown in Figure 3b, the FePt NSs increased to 5.70 mA cm^{-2}, which is 99.6% of the initial currents, and the FePt NPs increased to 5.15 mA cm^{-2}, which is 97.7% of the initial currents while the Pt/C only recovered 85.1% of its initial value. Moreover, when the gas was switched to O_2, the current density of the FePt NSs recovered to the limited currents more quickly than that of the FePt NPs and Pt/C electrodes based on the slopes of their $i-t$ curves in Figure 3b. These results indicate better CO tolerance from the FePt NSs than FePt NPs and the commercial Pt/C. To further prove this result, the ORR polarization curves were also carried out prior to and post CO-tolerance experiments (Figure 3c,d). For the FePt NSs, the ORR curves coincided well before and after the CO-tolerant experiment. Accordingly, the mass activity still held 95.38% after CO-tolerance experiments (Figure 3d). On the contrary, for the FePt NPs, the mass activity only recovered 72.01%, and, for Pt/C, only 13.76% activity recovered. The ORR curve of Pt/C shifted obviously toward the negative potential, which is poor in CO-tolerant performance. Thus, the ORR mass activity of FePt NSs showed 49.1 times higher than that of Pt/C after CO poisoning.

The effect of CO on the electrocatalytic activity of the electrode was also tested with the addition of CO in the O_2-saturated electrolyte by $i-t$ chronoamperometric response to give more intuitive effects. The FePt NS was the most tolerant to CO poisoning with only a 5% loss in current density even after mixing 10% CO with O_2 gas (Figure 3g), whereas the FePt NP decreased more (about 11%) in current density and the Pt/C electrode was rapidly poisoned under the same condition with a sharp decrease of current density (~34%) (Figure 3g). These results also indicate that beyond the significantly improved electrocatalytic activity, the FePt NS catalysts also demonstrated outstanding consistency and stability, which is another major improvement toward fuel cell application with air as the oxygen resource. This high resistance to CO poisoning can be revealed by the CO stripping curves in Figure 3h. The peak potential of adsorbed CO (CO_{ads}) electrooxidation on the FePt NSs catalyst is 0.690 V, which negatively shifted by 43 mV compared with that of the Pt/C catalyst at 0.733 V. Furthermore, the peak current density of CO_{ads} is much smaller than that of Pt/C, which indicates the low coverage of CO on the surface. FePt NPs also showed a very weak CO_{ads} electrooxidation peak due to the low coverage of CO_{ads} on the surface of FePt NPs with less than 10% containing Pt atoms and the smaller peak than NSs maybe result from their 3D sphere structure, where lots of the Pt atoms are located inside rather than on the surface. These results indicate that the FePt nanostructures have a much higher tolerance toward CO_{ads} poisoning.

It is widely accepted that in Pt-based intermetallic Pt−M (M = Ni, Fe, Co) catalysts, the promotional effect of M for the CO oxidation reaction comes from the activation of oxygen atoms on M sites[60,61] and the decrease in the adsorption energy of CO over the neighboring Pt surfaces.[55,62] To investigate the origination of the enhanced CO tolerance of the FePt NS catalyst, the DFT calculations were further employed to investigate the adsorption energy of the related CO and OH species on the FePt and pure Pt surfaces (Figure 4). As shown in Figure 4 and Table S3, the adsorption energy of CO (ΔE_{CO}) on the FePt (111) surface is calculated to be −1.63 eV on fcc site, which is smaller than that on a pure Pt(111) surface (−1.73 eV). This difference in ΔE_{CO} indicated the weakened CO bonding on the FePt surface compared to that on the Pt

DOI: 10.1021/acs.nanolett.8b02606
Nano Lett. XXXX, XXX, XXX−XXX

surface.[63,64] According to the calculated density of states (DOS) (Figure 4a,b), the weakened CO bonding to FePt(111) could be related to the downshifting of the d band center of the Pt atom compared to Pt(111), leading to a smaller energy separation between the Pt d band and CO p orbital, which results in the decrease of an electron back-donation, in agreement with the previous report.[63] In addition, almost all other sites of FePt exhibited a markedly lower adsorption energy than the pure Pt, which further proved its weak CO bonding (Figure 4c,d and Table S3). OH adsorption energy (ΔE_{OH}) on the FePt (111) surface was −4.66 eV on the most stable hcp sites (composed by three Fe atoms, marked by number "8" in Figure 4e), while ΔE_{OH} on pure Pt (111) was −2.32 eV indicating that the OH adsorption on the NSs is considerably stronger than that on pure Pt(111), which is consistent with our DOS plot (Figure S14). Therefore, it is likely to collect more OH species nearby the Fe, which is beneficial for the elimination of CO_{ads} on Pt.[65,66] Also, for Pt, a stronger OH adsorption is not beneficial to the ORR specific activity, and this is in agreement with our results that the specific area activity (i_s) of FePt NSs was lower than that of Pt/C. Even though, however, due to the highly efficient utilization and exposure of Pt sites, the overall mass activity could still be largely improved. On the other hand, the adsorption of OH on the Pt top site is weakened and the stronger OH adsorption is mainly from the surrounding Fe sites, but not Pt sites; henceforth, due to the beneficial adsorption on the nearby Fe atoms, the adsorption of OH on Pt sites would be suppressed because the repelling interaction effect and competitive relationship of Fe. Hence, this will also improve the performance of the overall ORR of FePt NSs. On the basis of these results, we can conclude that the high CO tolerance on FePt NSs originated from the decreased CO adsorption energy and the stronger interaction of CO intermediate with OH nearby. The Fe atom is beneficial for providing more OH groups to react with the CO at Pt sites, thus also facilitate the elimination of CO_{ads} through electrooxidation.

In summary, we report a facile, one-pot, bottom-up approach to produce FePt NSs with a few-atom-layers thick in a high yield (~95%), which contains "neighboring Pt atoms" with atomic dispersion in a high density. Different from the traditional single atom catalysts, these neighboring Pt atoms contained in bimetallic nanosheets showed an excellent electrocatalytic activity, an outstanding four-electron path, as well as an outstanding CO tolerance toward the ORR. This as-proofed "neighboring atoms catalyst" not only preserves the advantages of the traditional single atom catalysts but also can synergistically interact with oxygen to catalyze the reaction ,which needs two or more nearby sites. The CO tolerance arises from the downshifting of the Pt d band, which makes Pt interact weakly with the CO p orbital and hence decreases the adsorption and subsequently the coverage of CO over Pt. The extremely high specific surface area and performance come from the atomic dispersion and highly improved accessibility of Pt atoms on the surface. The novel 2D FePt ultrathin structure with a wrinkled surface also displayed the advantages of 2D materials in catalysis. The improved activity and neighboring atoms design in ultrathin 2D bimetallic materials pave the promising alternative road to traditional Pt-NP or isolated single atom-based electrocatalysts for the sustainable application toward the ORR catalysis in fuel cells.

■ ASSOCIATED CONTENT

Supporting Information

The Supporting Information is available free of charge on the ACS Publications website at DOI: 10.1021/acs.nanolett.8b02606.

Additional experimental procedures, calculation details on the estimation of specific surface area of Pt single atoms, detailed investigation of the formation of the FePt NSs, XRD, SEM and TEM images, HR-STEM, EDX mapping, durability test, and DOS, ICP, ORR performance, and DFT calculation results (PDF)

■ AUTHOR INFORMATION

Corresponding Authors

*E-mail: jianbowu@sjtu.edu.cn.
*E-mail: xiaoqing.pan@uci.edu.
*E-mail: hong.zhu@sjtu.edu.cn.

ORCID

Wen Shang: 0000-0002-6984-3060
Peng Tao: 0000-0002-9284-7158
Chengyi Song: 0000-0002-4757-9481
Tao Deng: 0000-0002-1560-3838
Hong Zhu: 0000-0001-7919-5661
Xiaoqing Pan: 0000-0002-0965-8568
Hong Yang: 0000-0003-3459-4516
Jianbo Wu: 0000-0002-3574-5585

Author Contributions

The manuscript was written through contributions of all authors. All authors have given approval to the final version of the manuscript. W.C. and W.G. contributed equally to this work.

Notes

The authors declare no competing financial interest.

■ ACKNOWLEDGMENTS

The work is sponsored by the thousand talents program for distinguished young scholars from the Chinese government, the National Key R&D Program of China (2017YFB0406000), and the National Science Foundation of China (51521004 and 51420105009) and the start-up fund (J.W.) and the Zhi-Yuan Endowed fund (T.D.) from Shanghai Jiao Tong University. W.G. and X.P. were supported by the National Science Foundation (CBET 1159240, DMR-1420620, and DMR-1506535). TEM work (on JEM 2800 and Grand ARM) was conducted using the facilities in the Irvine Materials Research Institute (IMRI) at the University of California, Irvine. We would like to acknowledge Qiaoshi Zeng (Center for High-Pressure Science & Technology Advanced Research) for Analysis and Characterization of the XAFS.

■ REFERENCES

(1) Ling, T.; Wang, J. J.; Zhang, H.; Song, S. T.; Zhou, Y. Z.; Zhao, J.; Du, X. W. *Adv. Mater.* **2015**, *27*, 5396−5402.
(2) Wu, J. B.; Yang, H. *Acc. Chem. Res.* **2013**, *46*, 1848−1857.
(3) Li, M.; Zhao, Z.; Cheng, T.; Fortunelli, A.; Chen, C.-Y.; Yu, R.; Zhang, Q.; Gu, L.; Merinov, B.; Lin, Z.; Zhu, E.; Yu, T.; Jia, Q.; Guo, J.; Zhang, L.; Goddard, W. A.; Huang, Y.; Duan, X. *Science* **2016**, *354*, 1414−1419.
(4) Wu, J. B.; Zhang, J. L.; Peng, Z. M.; Yang, S. C.; Wagner, F. T.; Yang, H. *J. Am. Chem. Soc.* **2010**, *132*, 4984−4985.
(5) Wu, J. B.; Gross, A.; Yang, H. *Nano Lett.* **2011**, *11*, 798−802.

DOI: 10.1021/acs.nanolett.8b02606
Nano Lett. XXXX, XXX, XXX−XXX

(6) Wang, Y. J.; Zhao, N. N.; Fang, B. Z.; Li, H.; Bi, X. T. T.; Wang, H. J. *Chem. Rev.* **2015**, *115*, 3433−3467.
(7) Ma, Y. L.; Gao, W. P.; Shan, H.; Chen, W. L.; Shang, W.; Tao, P.; Song, C. Y.; Addiego, C.; Deng, T.; Pan, X. Q.; Wu, J. B. *Adv. Mater.* **2017**, *29*, 1703460.
(8) Geim, A. K.; Grigorieva, I. V. *Nature* **2013**, *499*, 419−425.
(9) Du, Y. P.; Yin, Z. Y.; Zhu, J. X.; Huang, X.; Wu, X. J.; Zeng, Z. Y.; Yan, Q. Y.; Zhang, H. *Nat. Commun.* **2012**, *3*, 1177.
(10) Kuang, Y.; Feng, G.; Li, P. S.; Bi, Y. M.; Li, Y. P.; Sun, X. M. *Angew. Chem., Int. Ed.* **2016**, *55*, 693−697.
(11) Gao, S.; Lin, Y.; Jiao, X. C.; Sun, Y. F.; Luo, Q. Q.; Zhang, W. H.; Li, D. Q.; Yang, J. L.; Xie, Y. *Nature* **2016**, *529*, 68−71.
(12) Yan, J. Q.; Wang, T.; Wu, G. J.; Dai, W. L.; Guan, N. J.; Li, L. D.; Gong, J. L. *Adv. Mater.* **2015**, *27*, 1580−1586.
(13) Chhowalla, M.; Shin, H. S.; Eda, G.; Li, L. J.; Loh, K. P.; Zhang, H. *Nat. Chem.* **2013**, *5*, 263−275.
(14) Kalantar-zadeh, K.; Ou, J. Z.; Daeneke, T.; Strano, M. S.; Pumera, M.; Gras, S. L. *Adv. Funct. Mater.* **2015**, *25*, 5086−5099.
(15) Feng, J.; Peng, L. L.; Wu, C. Z.; Sun, X.; Hu, S. L.; Lin, C. W.; Dai, J.; Yang, J. L.; Xie, Y. *Adv. Mater.* **2012**, *24*, 1969−1974.
(16) Duan, H. H.; Yan, N.; Yu, R.; Chang, C. R.; Zhou, G.; Hu, H. S.; Rong, H. P.; Niu, Z. Q.; Mao, J. J.; Asakura, H.; Tanaka, T.; Dyson, P. J.; Li, J.; Li, Y. D. *Nat. Commun.* **2014**, *5*, 3093.
(17) Zhang, J. S.; Chen, Y.; Wang, X. C. *Energy Environ. Sci.* **2015**, *8*, 3092−3108.
(18) Jaramillo, T. F.; Jorgensen, K. P.; Bonde, J.; Nielsen, J. H.; Horch, S.; Chorkendorff, I. *Science* **2007**, *317*, 100−102.
(19) Deng, J.; Yuan, W. T.; Ren, P. J.; Wang, Y.; Deng, D. H.; Zhang, Z.; Bao, X. H. *RSC Adv.* **2014**, *4*, 34733−34738.
(20) Tongay, S.; Zhou, J.; Ataca, C.; Lo, K.; Matthews, T. S.; Li, J. B.; Grossman, J. C.; Wu, J. Q. *Nano Lett.* **2012**, *12*, 5576−5580.
(21) Zhao, L.; Xu, C. F.; Su, H. F.; Liang, J. H.; Lin, S. C.; Gu, L.; Wang, X. L.; Chen, M.; Zheng, N. F. *Adv. Sci.* **2015**, *2*, 1500100.
(22) Huang, X. Q.; Tang, S. H.; Mu, X. L.; Dai, Y.; Chen, G. X.; Zhou, Z. Y.; Ruan, F. X.; Yang, Z. L.; Zheng, N. F. *Nat. Nanotechnol.* **2011**, *6*, 28−32.
(23) Pan, Y. T.; Yin, X.; Kwok, K. S.; Yang, H. *Nano Lett.* **2014**, *14*, 5953−5959.
(24) Yin, A. X.; Liu, W. C.; Ke, J.; Zhu, W.; Gu, J.; Zhang, Y. W.; Yan, C. H. *J. Am. Chem. Soc.* **2012**, *134*, 20479−20489.
(25) Huang, X.; Li, S. Z.; Huang, Y. Z.; Wu, S. X.; Zhou, X. Z.; Li, S. Z.; Gan, C. L.; Boey, F.; Mirkin, C. A.; Zhang, H. *Nat. Commun.* **2011**, *2*, 292.
(26) Saleem, F.; Xu, B. A.; Ni, B.; Liu, H. L.; Nosheen, F.; Li, H. Y.; Wang, X. *Adv. Mater.* **2015**, *27*, 2013−2018.
(27) Hong, J. W.; Kim, Y.; Wi, D. H.; Lee, S.; Lee, S. U.; Lee, Y. W.; Choi, S. I.; Han, S. W. *Angew. Chem., Int. Ed.* **2016**, *55*, 2753−2758.
(28) Yan, Y.; Shan, H.; Li, G.; Xiao, F.; Jiang, Y.; Yan, Y.; Jin, C.; Zhang, H.; Wu, J.; Yang, D. *Nano Lett.* **2016**, *16*, 7999−8004.
(29) Bu, L.; Zhang, N.; Guo, S.; Zhang, X.; Li, J.; Yao, J.; Wu, T.; Lu, G.; Ma, J.-Y.; Su, D.; Huang, X. *Science* **2016**, *354*, 1410−1414.
(30) Chhetri, M.; Rana, M.; Loukya, B.; Patil, P. K.; Datta, R.; Gautam, U. K. *Adv. Mater.* **2015**, *27*, 4430−4437.
(31) Wang, X.; Choi, S.-I.; Roling, L. T.; Luo, M.; Ma, C.; Zhang, L.; Chi, M.; Liu, J.; Xie, Z.; Herron, J. A.; Mavrikakis, M.; Xia, Y. *Nat. Commun.* **2015**, *6*, 7594.
(32) Wu, J. B.; Qi, L.; You, H. J.; Gross, A.; Li, J.; Yang, H. *J. Am. Chem. Soc.* **2012**, *134*, 11880−11883.
(33) Cui, C.; Gan, L.; Heggen, M.; Rudi, S.; Strasser, P. *Nat. Mater.* **2013**, *12*, 765−771.
(34) Wang, J. X.; Inada, H.; Wu, L. J.; Zhu, Y. M.; Choi, Y. M.; Liu, P.; Zhou, W. P.; Adzic, R. R. *J. Am. Chem. Soc.* **2009**, *131*, 17298−17302.
(35) Xiong, Y.; Shan, H.; Zhou, Z.; Yan, Y.; Chen, W.; Yang, Y.; Liu, Y.; Tian, H.; Wu, J.; Zhang, H.; et al. *Small* **2017**, *13*, 1603423.
(36) Smith, A. J.; Chang, Y. H.; Raidongia, K.; Chen, T. Y.; Li, L. J.; Huang, J. *Adv. Energy Mater.* **2014**, *4*, 1400398.
(37) Luo, J. Y.; Jang, H. D.; Huang, J. X. *ACS Nano* **2013**, *7*, 1464−1471.
(38) Yang, X. F.; Wang, A. Q.; Qiao, B. T.; Li, J.; Liu, J. Y.; Zhang, T. *Acc. Chem. Res.* **2013**, *46*, 1740−1748.
(39) Li, X. G.; Bi, W. T.; Zhang, L.; Tao, S.; Chu, W. S.; Zhang, Q.; Luo, Y.; Wu, C. Z.; Xie, Y. *Adv. Mater.* **2016**, *28*, 2427−2431.
(40) Liu, J.; Jiao, M. G.; Lu, L. L.; Barkholtz, H. M.; Li, Y. P.; Wang, Y.; Jiang, L. H.; Wu, Z. J.; Liu, D. J.; Zhuang, L.; Ma, C.; Zeng, J.; Zhang, B. S.; Su, D. S.; Song, P.; Xing, W.; Xu, W. L.; Wang, Y.; Jiang, Z.; Sun, G. Q. *Nat. Commun.* **2017**, *8*, 15938.
(41) Yang, S.; Kim, J.; Tak, Y. J.; Soon, A.; Lee, H. *Angew. Chem., Int. Ed.* **2016**, *55*, 2058−2062.
(42) Choi, C. H.; Kim, M.; Kwon, H. C.; Cho, S. J.; Yun, S.; Kim, H. T.; Mayrhofer, K. J. J.; Kim, H.; Choi, M. *Nat. Commun.* **2016**, *7*, 10922.
(43) Yan, H.; Lin, Y.; Wu, H.; Zhang, W. H.; Sun, Z. H.; Cheng, H.; Liu, W.; Wang, C. L.; Li, J. J.; Huang, X. H.; Yao, T.; Yang, J. L.; Wei, S. Q.; Lu, J. L. *Nat. Commun.* **2017**, *8*, 1070.
(44) Gong, K. P.; Du, F.; Xia, Z. H.; Durstock, M.; Dai, L. M. *Science* **2009**, *323*, 760−764.
(45) Zhang, M.; Dai, L. M. *Nano Energy* **2012**, *1*, 514−517.
(46) Wang, S.; Iyyamperumal, E.; Roy, A.; Xue, Y.; Yu, D.; Dai, L. *Angew. Chem., Int. Ed.* **2011**, *50*, 11756−11760.
(47) Liu, Z.; Jackson, G. S.; Eichhorn, B. W. *Energy Environ. Sci.* **2011**, *4*, 1900−1903.
(48) Sun, X.; Zhang, Y.; Song, P.; Pan, J.; Zhuang, L.; Xu, W.; Xing, W. *ACS Catal.* **2013**, *3*, 1726−1729.
(49) Adler, S. B. *Chem. Rev.* **2004**, *104*, 4791−4843.
(50) Wen, Z. H.; Liu, J.; Li, J. H. *Adv. Mater.* **2008**, *20*, 743−747.
(51) Shao, M. H.; Chang, Q. W.; Dodelet, J. P.; Chenitz, R. *Chem. Rev.* **2016**, *116*, 3594−3657.
(52) Liu, Z. F.; Jackson, G. S.; Eichhorn, B. W. *Energy Environ. Sci.* **2011**, *4*, 1900−1903.
(53) Ehteshami, S. M. M.; Chan, S. H. *Electrochim. Acta* **2013**, *93*, 334−345.
(54) Wei, H. S.; Liu, X. Y.; Wang, A. Q.; Zhang, L. L.; Qiao, B. T.; Yang, X. F.; Huang, Y. Q.; Miao, S.; Liu, J. Y.; Zhang, T. *Nat. Commun.* **2014**, *5*, 5634.
(55) Deng, D. H.; Novoselov, K. S.; Fu, Q.; Zheng, N. F.; Tian, Z. Q.; Bao, X. H. *Nat. Nanotechnol.* **2016**, *11*, 218−230.
(56) Wang, R. Y.; Liu, J. G.; Liu, P.; Bi, X. X.; Yan, X. L.; Wang, W. X.; Ge, X. B.; Chen, M. W.; Ding, Y. *Chem. Sci.* **2014**, *5*, 403−409.
(57) Greeley, J.; Stephens, I. E. L.; Bondarenko, A. S.; Johansson, T. P.; Hansen, H. A.; Jaramillo, T. F.; Rossmeisl, J.; Chorkendorff, I.; Norskov, J. K. *Nat. Chem.* **2009**, *1*, 552−556.
(58) Chen, S.; Bi, J. Y.; Zhao, Y.; Yang, L. J.; Zhang, C.; Ma, Y. W.; Wu, Q.; Wang, X. Z.; Hu, Z. *Adv. Mater.* **2012**, *24*, 5593−5597.
(59) Birry, L.; Zagal, J. H.; Dodelet, J. P. *Electrochem. Commun.* **2010**, *12*, 628−631.
(60) Fu, Q.; Li, W. X.; Yao, Y. X.; Liu, H. Y.; Su, H. Y.; Ma, D.; Gu, X. K.; Chen, L. M.; Wang, Z.; Zhang, H.; Wang, B.; Bao, X. H. *Science* **2010**, *328*, 1141−1144.
(61) Kotobuki, M.; Watanabe, A.; Uchida, H.; Yamashita, H.; Watanabe, M. *J. Catal.* **2005**, *236*, 262−269.
(62) Nilekar, A. U.; Alayoglu, S.; Eichhorn, B.; Mavrikakis, M. *J. Am. Chem. Soc.* **2010**, *132*, 7418−7428.
(63) Xu, C. X.; Li, Q.; Liu, Y. Q.; Wang, J. P.; Geng, H. R. *Langmuir* **2012**, *28*, 1886−1892.
(64) Watanabe, M.; Zhu, Y. M.; Uchida, H. *J. Phys. Chem. B* **2000**, *104*, 1762−1768.
(65) Liu, P.; Logadottir, A.; Norskov, J. K. *Electrochim. Acta* **2003**, *48*, 3731−3742.
(66) Gasteiger, H. A.; Markovic, N.; Ross, P. N.; Cairns, E. J. *J. Phys. Chem.* **1994**, *98*, 617−625.

DOI: 10.1021/acs.nanolett.8b02606
Nano Lett. XXXX, XXX, XXX−XXX